Crosswell Seismic Imaging In A Contaminated Basalt Aquifer - Final Report

LBNL Research Report LBNL-45533

Thomas M. Daley, Ernest L. Majer and John E. Peterson

Lawrence Berkeley National Laboratory

Short title: CROSSWELL SEISMIC IN BASALT

Abstract. Multiple seismic crosswell surveys have been acquired and analyzed by LBNL in a fractured basalt aquifer at Idaho National Engineering and Environmental Laboratory (INEEL). Most of these surveys used a high frequency (1000 - 10,000 Hz) piezoelectric seismic source to obtain P-wave velocity tomograms. Additionally, we deployed a new type of borehole seismic source as part of the subsurface characterization program at a contaminated groundwater site. This source, know as an orbital vibrator, allows simultaneous acquisition of P- and S-waves at frequencies of 100 to 400 Hz. The orbital vibrator was developed for oil field applications and, to our knowledge, this is the first environmental application. Both velocity and attenuation tomograms have been calculated. The velocity tomograms show a relationship to contaminant transport in the groundwater (as measured by logs and cores). Zones of high contaminant flux are coincident with zones of low velocity (both P- and S-wave) and high attenuation. We believe horizontal fracture zones at the boundaries of basalt flows are controlling the contaminant flow and we have imaged these zones with seismic properties (velocity and attenuation). The lower resolution of the orbital vibrator data was sufficient for constraining hydrologic models while achieving imaging over larger interwell distances. We used the P- and S-wave data to calculated Vp/Vs and we have used an equivalent media approximation to calculate fracture density within the aquifer. Additionally, high amplitude guided waves are observed and numerically modeled. We believe these waves delineate thin (1-2 m) zones of velocity contrast which indicate fracturing and, in this instance, delineate a permeable fracture zone with high contaminant flow.

1. INTRODUCTION

The remediation of contaminated aquifers is important to the long-term health of water supplies. Designing appropriate remediation strategies (such as bioremediation or pump-and-treat) requires an understanding of aquifer properties and the subsurface structure which controls those properties. Seismology provides important methods for imaging subsurface structure. Seismic reflection imaging, using surface sources and receivers has been widely used, however the resolution of subsurface features is limited by the seismic wavelength. The need for higher resolution imaging has led to borehole seismic techniques which place sources and sensors at depth in wells and generate shorter wavelengths. One important method for borehole seismology is crosswell tomography. Crosswell seismic surveys have been used for many years to tomographically image P-wave velocity between wells (e.g. [Mason, 1981] and [Peterson, et al., 1985]). More recently, crosswell S-waves have also been used to map S-wave velocity [Harris, et al., 1995] and both P- and S-wave crosswell reflectivity have been analyzed for structural delineation [Rector et al., 1995].

Most crosswell seismic tomography has been performed in sedimentary formations important to oil and gas exploitation [Rector et al., 1995]. However, some of the important aquifer contamination problems occur in crystalline rock, such as the Snake River Plain basalt aquifer in Idaho. The application of crosswell seismic methods to crystalline rock is often a more difficult problem than the application to sedimentary rock. In crystalline rock, the features important to fluid flow are usually fractures.

Fractures in rocks can cause large seismic velocity and amplitude changes compared to the intact matrix. Various approaches have been taken to develop theory to relate these changes to fracture properties (e.g. [O'Connell and Budiansky, 1974], [Pyrak-Nolte, et al., 1990], [Schoenberg and Sayers, 1995]). However, other subsurface features such as matrix heterogeneity, fluid saturation and partial gas saturation make direct measurement of fracture properties difficult in practice. Without attempting to directly invert for fracture properties, the seismic attributes (e.g. velocity and attenuation) can be related to subsurface features determined from borehole methods such as core analysis and well logs. The advantage of seismic imaging is the ability to detect or image features away from the borehole. Crosswell seismic imaging in fractured crystalline rock has been used to define the spatial distribution of velocity and attenuation, which are related to fracture zones determined from other borehole techniques (e.g. [Vasco, et al., 1996], [Cao and Greenhalgh, 1997]).

As part of a U.S. Department of Energy research program (the Environmental Management Science Program), we conducted crosswell seismic studies at the Idaho National Engineering and Environmental Laboratory (INEEL). At INEEL, we have applied the crosswell seismic technique in a fractured basalt aquifer (part of the Snake River Plain Aquifer) which has been locally contaminated by historic injection of waste into a disposal well at the Test Area North (TAN) site (as described in the next section). Multiple crosswell surveys were acquired in two field sessions. The initial surveys used a piezoelectric source which provided high frequency (1000 - 10,000 Hz), high resolution P-wave data. The second field session used an orbital vibrator source which generates

lower frequency (70-400 Hz), higher amplitude P-waves, thereby allowing more spatial coverage (larger well spacings) albeit with lower resolution than the piezoelectric source data. The orbital vibrator is also notable for generating S-waves as well as P-waves, thereby providing a separate measure of rock properties.

Our analysis of the crosswell data includes imaging of fracture zones important for fluid flow and contaminant transport. Zones with fracture flow of contaminants are inferred from well logs and core sampling. Velocity and attenuation tomograms for the piezoelectric source data image apparent fracture flow zones with about 1 - 2 m resolution. P- and S-wave velocity tomograms for the orbital vibrator source both have 10 - 15 m resolution of zones with high apparent contaminant flow. The combined P and S-Wave measurements are used to estimate fracture density. Also, a guided wave, generated by the orbital vibrator, is detected in a zone observed to have fracture flow. The guided wave is numerically modeled to estimate layer thickness with about 1 m resolution.

2. Field Site, Data Acquisition and Processing

The INEEL lies on the eastern half of the Snake River Plain in southern Idaho. The geohydrologic framework has been described by Whitehead (1992). The eastern plain is underlain by Quaternary age basalt of the Snake River Group with some sedimentary interbedding. The basalt section can be as over 1.5 km thick. The eastern plain has a sequence of thin-layered basalt flows which can yield large volumes of groundwater. The TAN site of INEEL overlies a portion of the Snake River Plain aquifer where the

saturated thickness is about 180 m, and basalt flows are interspersed with sedimentary interbeds. The TAN site has mixed waste contamination including TCE, PCE, DCE and radionuclides believed to originate from a waste injection well (TSF-05 in Figure 1). The contaminant plume is in the saturated zone of the aquifer which begins at about 60 m below ground level. From the water table down to about 98 m, the aquifer appears to consist of numerous thin (1 - 6 m) basalt flows, with a thick flow below 100 m which limits downward migration of contaminants. A conceptual model of the site showing flow and barrier zones within the series of basalt flows is shown in Figure 2. The hydrologic flow conditions and contaminant distribution at TAN have been described in a series of site reports ([Bukowski and Sorenson, 1998], [Bukowski, et al., 1998], [Sorenson, et al., 1996]). The most detailed measurement of contaminant distribution, particularly the vertical distribution, has been obtained from gamma logs. The gamma logs respond to trace amounts of radionuclides present in the contaminant source and are used to infer the presence of contaminated ground water. Figure 3 shows a series of gamma logs for wells at the TAN site used for seismic tomography. The seismic imaging focused on the 60 to 90 m depth zone of the aquifer. The upper portion of this zone (approximately 60 to 75 m) contains the majority of contamination as shown by the dotted lines in Figure 3.

A large part of the hydrologic research for site remediation is focused on determining the scale at which the aquifer can be treated as an equivalent porous medium for numerical modeling [Bukowski and Sorenson, 1998]. Two types of seismic sources were able to define different scale lengths. The initial borehole seismic acquisition used a high

frequency piezoelectric source. The success of this technique in defining thin zones in the upper, high-flow section was limited only by the distances which could be surveyed because of attenuation of the seismic signal. A follow-up survey was performed using an orbital vibrator, a more powerful, lower frequency seismic source which was successful in obtaining data over larger distances between wells while still differentiating between the upper (60 -75 m), high-flow portion of the aquifer and the lower (75 -90 m), low-flow portion of the aquifer.

2.1. Piezoelectric Source Acquisition

In November 1996, LBNL acquired seismic cross-well data at the TAN site using a high frequency (1000 - 10,000 Hz) piezoelectric source along with commercial borehole hydrophone sensors. The source and sensors were stationed every 0.5 m from the water table (approximately 65 m) to 100 m (or to the well bottom). While high quality piezoelectric data was obtained from 5 well pairs (Figure 1), limited propagation distance (about 25 m maximum) of the high frequency waves restricted the areal extent of our imaging. Other well pairs were attempted, but we did not obtain data usable for tomography. A summary of all piezoelectric source acquisition at the TAN site (including the unsuccessful attempts) is shown in Table 1.

Table 1.

Source Well	Receiver Well	Data Quality	Tomogram Generated
TAN-31	TAN-9	Good	Yes
TAN-25	TAN-26	Good	Yes
TAN-25	TAN-31	Fair	Yes (below 80 m only)
TAN-25	TSF-05	Fair	Yes
TAN-31	TSF-05	Poor	No
TAN-31	TAN-26	Poor	No
TAN-9	TAN-26	Poor	No
TAN-19	TAN-18	Good	Yes
TAN-19	USGS-24	Bad	No
TAN-19	TAN-33	Poor	No
USGS-24	TAN-33	Bad	No

Table 1: Piezoelectric Data Acquisition

The total seismic attenuation (including intrinsic and scattered loses), observed as variations in acquisition signal-to-noise ratio (assuming constant background noise), did vary spatially; localized high attenuation limited propagation at certain depths for some well pairs. For example, the TAN-31 and TAN-25 well pair acquisition provided usable data below 80 m, but not above 80 m with the same source-receiver separation. In general, the piezoelectric source could only propagate usable energy about 20 m between

wells, with some zones having poor data at well spacing of 10 - 15 m. Usable energy is defined as providing signal-to-noise ratios sufficient for first arrival identification.

2.2. Piezoelectric Data Processing

Despite limitations on propagation distance (which exist for any site and any seismic source), the piezoelectric source data at TAN are generally good quality. Figure 4a shows an example set of crosswell seismic recordings. The source is impulsive (similar to an explosive source) and the arrival time of the fastest seismic wave is picked at the point at which the waveform emerges from the background noise. Prior to picking arrival times, the data processing consists of summing multiple shots of the source (typically about 25 shots) and filtering the broadband digital recordings to the frequency band of the seismic energy (typically 800 to 8000 Hz).

After picking the arrival times, various checks on quality and consistency of picks are made including analyzing travel time versus distance and travel time versus source-receiver offset. Times found to be in error (mispicked) are repicked or removed from the travel time data set. The remaining travel times are used for tomographic inversion. The inversion used is an algebraic reconstruction technique (ART) described by [Peterson, et al., 1985]. This algorithm uses straight raypaths between source and sensor locations, divides the subsurface into a 2-D grid between wells. The 2-D cross-section between wells is divided into square cells (0.5 m^2 for TAN data) and the seismic velocity is estimated in each cell. The relation between total travel time, t_k, and

the 2D medium velocity, $v(x,y)$, is given by

$$t_k = \int_{R_k} \frac{ds}{v(x,y)} \tag{1}$$

for a segment s of the k^{th} raypath R_k. Similarly, the seismic attenuation can be imaged by relating the recorded amplitude, A_k, to the 2D attenuation structure, $\alpha(x,y)$ through the equation

$$A_k = A_0 e^{\left[-\int_{R_k} \alpha(x,y)ds\right]}, \tag{2}$$

and the function P_k, where

$$P_k = ln\frac{A_k}{A_0} = -\int_{R_k} \alpha(x,y)ds \tag{3}$$

where $\alpha(x,y) = \frac{\pi f}{cQ}$ for frequency f, velocity c, and attenuation factor Q. A_0 is the source amplitude corrected for radiation pattern, geometric spreading and instrument response. In general, the problem is written

$$y_k = \int_{R_k} x(r,s)ds \tag{4}$$

with y_k representing the measured traveltime or amplitude for k=1,...,N paths and x representing the slowness or attenuation operator. The problem is then discretized as a set of linear equations

$$y_k = \sum_{i=1}^{I} \delta\gamma_{ki} x_i \quad k = 1, ..., N \tag{5}$$

where $\delta\gamma_{ki}$ is the length of the ray k which penetrates pixel i, and I is the total number of pixels intersected by the ray k and x_i is the property of pixel i. The solutions are iterative and require an initial velocity model or begin with simple back-projection of

the data. The resolution of velocity in each cell is dependent on the seismic ray density and weights can be used to allow for varying ray-length in each cell [Peterson, et al., 1985].

Determining the relative depths and horizontal offsets of each source and receiver location (station) is very important to the inversion. Errors in location can induce apparent static shifts in velocity for a given station. These errors can be due to borehole deviation which was measured incorrectly or not measured at all, and survey errors in the borehole elevation. Also important is correcting for borehole effects such as change in borehole diameter or mechanical properties of the rock immediately surrounding the borehole. Drilling-induced fracturing can alter rock properties as a function of depth. This effect will also provide a static shift in the measured travel time for a given station. In our inversion, the travel time data are simultaneously inverted for static shifts at each source and receiver station as well as for the velocity field. This method is described in [Vasco, et al., 1996]. The resulting tomograms for the piezoelectric source data are shown in Figure 5 and will be discussed in the following sections.

The TAN-31 - TAN-9 data set has also been inverted for attenuation. In this analysis the amplitude of the first arrival, in a constant length time window, is computed for each seismic trace that has sufficient signal-to-noise ratio. The 2-D cross section between wells is then divided into pixels and each pixel is inverted for amplitude attenuation in dB/m. Seismic amplitudes are affected by many factors including the velocity structure, but they can provide useful information in a fractured aquifer [Vasco, et al., 1996]. Figure 6 shows the attenuation and velocity tomograms for the TAN-31 -

TAN-9 well pair. Both tomograms show horizontal features with low velocity associated with high attenuation, as predicted by most models of seismic wave propagation in fractures. The resolution of features in both tomograms is on the order of 1 to 2 m.

2.3. Orbital Vibrator Source Acquisition

In 1997 a new well was drilled at the TAN site. Because the crosswell distances to this well, TAN-37, were too long to acquire piezoelectric source data (because of seismic attenuation) our desire to image around this new well led us to consider the orbital vibrator seismic source which has higher energy output and lower frequency content than our piezoelectric source. The orbital vibrator is a mechanical borehole seismic source designed for oil and gas exploration [Daley and Cox, 1999]. Our DC powered version of the orbital vibrator runs on a standard 7-conductor armored cable. It has recorded data in sedimentary formations with well spacings over 300 m. The orbital vibrator also has the notable advantage of generating P- and S-wave energy simultaneously. While the lower frequency content (70 to 400 Hz) lowers the potential spatial resolution, it also increases the propagation distance in material of a given attenuation. Tests at the TAN site during orbital vibrator acquisition showed it could acquire data up to 57 m between wells TAN-37 and TAN-31. At this distance, the survey aperture (ratio of available well depth to well separation) becomes the limiting factor. An aperture of less than one results in significant degradation of tomographic resolution.

Orbital vibrator data was successfully acquired in two well pairs using TAN-37 as a source borehole (Figure 1), thereby extending the range of crosswell seismic surveys in

the fractured basalt aquifer of the TAN site. We show in Figure 4b typical recordings from the TAN-37 - TAN-25 well pair. The well separation was 38 m. The orbital vibrator acquisition also proved successful in acquiring P- and S-wave data using fluid-coupled hydrophone sensors. This represents the first use of hydrophone sensors with an orbital vibrator and demonstrates a more economical survey technique because hydrophones typically have more sensors per cable and faster acquisition than clamping borehole geophones. Because the orbital vibrator source is also fluid coupled, (with no clamping required) data acquisition within aquifers is very efficient.

One significant result of the orbital vibrator survey was the demonstration of S-wave crosswell acquisition with fluid coupled sources and sensors. The relatively high amplitude of S-waves generated (see Figure 4b) can overcome the reduced sensitivity of hydrophones (which sense the fluid pressure pule converted from incident S-waves) as compared to wall-locking sensors which directly measure S-waves. With the acquisition of an S-wave crosswell survey, in addition to the standard P-wave survey, significant additional information about subsurface materials can be inferred.

2.4. Orbital Vibrator Processing

The orbital vibrator seismic source requires a unique processing sequence (described in [Daley and Cox, 1999]) including source signal deconvolution and vector decomposition. The result is two data sets containing energy in the plane of the boreholes and energy normal to that plane. These data have separation of the P- and S-waves (where the S-wave is an SH type polarization for a vertical borehole).

Figure 4b shows the two data sets for a single receiver location. The travel times are picked and analyzed with the same method described above for the piezoelectric source. Attenuation tomography is possible with the orbital vibrator data, but it was not within the scope of this project.

The tomographic velocity inversion of the orbital vibrator data for wells TAN-37 and TAN-25 was performed for both P- and S-wave velocities using the procedures described for the piezoelectric source data. Figure 7 shows the P- and S-wave tomograms. The resolution of small features is worse than with the piezoelectric source, however the dominant feature of low velocities between 65 and 80 m is well delineated in both tomograms. Furthermore, the well spacing used for the orbital vibrator data was too large for the piezoelectric source which has less initial amplitude and more attenuation. Therefor, the orbital vibrator is an appropriate source for larger scales of investigation.

The orbital vibrator data for wells TAN-37 and TAN-30a was processed identically as for wells TAN-37 and TAN-25. However, there was a strong tube wave recorded in well TAN-30a. A tube wave is a type of surface wave at the borehole wall in fluid filled boreholes [White, 1965]. The tube-wave typically has large amplitude and a velocity near the shear-wave velocity. The tube-wave will also have multiple reflections from the well bottom and the water table. While some work has been done to use tube-wave properties to estimate rock properties near the borehole (e.g. [Cicerone and Toksoz, 1995]), for our tomographic imaging the tube-wave is coherent seismic noise. The tube wave is generated at certain depths when the P-wave is incident on the receiver borehole (TAN-30a), often arriving at the same time as the S-wave. Because of the tube-wave

noise in well TAN-30a, we only processed the P-wave travel time picks for the TAN-37 and TAN-30a well pair.

The two orbital vibrator tomograms form an image spanning wells TAN-25 to TAN-37 to TAN-30a. These two P-wave tomograms are shown in Figure 8 along with a borehole televiewer log [Bukowski, et al., 1998] from well TAN-37.

3. Interpretation

3.1. Piezoelectric Data Results

High quality P-wave arrivals were obtained with the piezoelectric seismic source at the TAN site over much of the 65 to 100 m survey depths. Seismic attenuation limited data quality in some depth zones. The travel time measurements were used to generate 5 crosswell tomograms, four of which are in the contaminant "hot spot" and are shown in Figure 5. We believe the observed velocity variations are due to material property variations of the basalt flows. During inspection of data gathers (eg Figures 4a and 4b), we did not observe coherent reflections which would indicate sedimentary interbeds in the depth range of our survey. We expect a sediment-basalt contact to be a laterally coherent reflector which would be observed in crosswell data.

We had hopped that tomograms from different well pairs would have similar features (which could be related to laterally continuous basalt flows, fracture zones or sedimentary interbeds), and we believe the resulting consistency between the 4 tomograms shown in Figure 5 is quite good. In Figure 5 we have interpreted 3 low

velocity zones as inferred fracture flow zones and one high velocity zone as an inferred flow barrier zone. This interpretation is based on the hypothesis that velocity is controlled by fracturing (or rubble between flows) with higher velocity corresponding to less fractured rock. As the rock fracture density increases, fracture permeability should increase.

We believe the tomograms show predominantly horizontal stratification which is best interpreted as independent basalt flows. We interpret the upper (66 - 68 m) and lower (85 - 87 m) low velocity zones as single interflow fracture/rubble zones. We interpret the center (73 - 78 m) low velocity zone of the TAN-31 - TAN-9 tomogram as two interflow zones with a thin (about 1 m) basalt flow in the middle at 76 - 77 m. This interpretation is supported by the TAN-25 - TAN-26 tomogram in which only the upper low velocity zone (74 -75 m) is well defined. In general, the features on the piezoelectric tomograms can be interpreted for interfaces and features of about 1 m thickness. We consider these interpretations on the 1 m scale to be the spatial limit of interpretability. Lateral resolution generally is not as good as the vertical resolution for crosswell acquisition geometry (Peterson, 1985), so changes within horizons between wells are less interpretable.

The TAN-25 - TAN-31 tomogram has slightly lower velocities in the lower (below 80 m) section, along with the high attenuation in the upper section (above 80 m) which prevented tomographic analysis. Low velocity and high attenuation can be caused by increased fracture content, borehole effects, as well as by increased TCE (or other dense nonaqueous phase liquid (DNAPL)) concentration and increased partial gas

saturation [Geller and Myer, 1995]. Borehole effects can be ruled out as the cause of high attenuation because both TAN-25 and TAN-31 were used in other tomograms which had higher velocity and lower attenuation. Therefor, we believe the tomograms are imaging lateral variations in fracture properties and/or saturating fluid properties.

The best measure of contaminant distribution in the TAN site wells is currently provided by gamma logs which show the response of radionuclide contamination (Figure 3). It is assumed that the organic contaminant flow is in the same zones as the radionuclide flow. Additionally, core samples from well TAN-37 have been analyzed for contaminants. The combination of well logs, core samples and crosswell imaging spans many scale lengths for estimating subsurface properties. Figure 9 shows a comparison of the gamma logs for well TAN-25 along with core samples of TCE concentrations from well TAN-37 and the crosswell tomograms. The gamma logs and the core samples confirm the presence of two flow zones at about 66 and 74 m. While these individual zones are not imaged by the orbital vibrator data, the piezoelectric tomograms (Figure 5) do image this zone. The deeper flow zone interpreted from the tomograms does not show increased aquifer contamination. Our interpretation of this observation is that the barrier zone interpreted on the piezoelectric tomograms is a dense, minimally fractured basalt acting as a barrier to vertical flow and therefor preventing significant contamination migration.

3.2. Orbital Vibrator Data Results

The lower frequency content of the orbital vibrator source leads to lower resolution of subsurface velocity structures. Figure 7 shows the P- and S-wave tomograms for TAN-25 - TAN-37, while figure 8 shows the P-wave tomograms along with the borehole televiewer data from well 37. The upper two low velocity zones identified with the piezoelectric source data are undelineated in the TAN-25 - TAN-37 tomogram and delineated somewhat better in the TAN-37 - TAN-30a tomogram. While the orbital vibrator data does not provide the 1 - 2 m resolution of the piezoelectric data because of its longer wavelength, it does image the lower velocities of the upper aquifer section (above 80 m). This resolution of the upper aquifer section is consistent with the scale required for hydrologic modeling of the TAN site [Bukowski, et al., 1998]. This consistency is important because the lower frequency content, coupled with higher output energy, did lead to imaging over larger distances. The attempt of 35 to 40 m well separations for the two cross-sections was successful, and a test recording between wells TAN-37 and TAN-31 showed usable arrivals at a distance of 57 m. Thus, the subsurface heterogeneity which impacts the hydrologic models can be monitored by seismic tomography at these distances. The important hydrologic parameter of scale for equivalent porous media calculations at the TAN site is sufficiently matched with the lower resolution orbital vibrator data (John Bukowski, pers comm, 1999).

3.2.1. Vp/Vs and Fracture Density Estimates. The consistent generation of P- and S-waves by the orbital vibrator source allows direct measurement of Vp/Vs

ratio. This ratio, along with the related Poisson's ratio, is an important parameter in rock physics because, for a given density, Vs is controlled by the rock matrix while Vp is controlled by both the matrix and the pore/fracture filling material. Figure 10 shows a Vp/Vs tomograms generated for the TAN-37 - TAN-25 well pair. The Vp/Vs ratio has a wide range of values from below 1.8 to over 2.8. These are generally high values compared to a typical Poisson solid (Vp/Vs = 1.73). We beleive these high Vp/Vs ratios indicate fracturing of the basalt. The Vp/Vs ratio was generated from independent inversions of P- and S-wave velocity. A more accurate estimate may be obtained by direct inversion the of P- and S-wave travel time ratio.

3.2.2. Crack Density Estimate. Because we believe the wave propagation at the TAN site is largely controlled by fracture properties, we applied fracture-based estimates of P- and S-wave velocity to the orbital vibrator data. The data is low frequency, and hence long wavelength, compared to fracture size. We also expect fairly random orientation of fractures. Therefore we decided to estimate rock properties using an equivalent media description of fractures [O'Connell and Budiansky, 1974]. This model is appropriate for our situation of long wavelengths (about 10 m) compared to fracture size (presumably 0.1 to 1 m). In the O'Connell and Budiansky model, the effect of thin randomly-oriented ellipsoidal cracks with variable saturation on material properties is calculated as though there is a media having equivalent properties to the fractured solid.

The crack density, ϵ, is defined by $\epsilon = (2N/\pi)(A^2/P)$, where N = cracks per unit volume, A is the area of a crack, and P is the perimeter. This relationship for a partially

saturated cracked rock is given by

$$\epsilon = \frac{45}{16}\frac{(\nu - \bar{\nu})}{(1 - \bar{\nu}^2)}\frac{(2 - \bar{\nu})}{[(1 - \xi)(1 + 3\nu)(2 - \bar{\nu}) - 2(1 - 2\nu)]} \tag{6}$$

where ϵ = the crack density, ν = Poisson's ratio for the uncracked matrix, $\bar{\nu}$ = Poisson's ratio for the cracked rock, and ξ = fraction of cracks which are saturated.
We assumed full saturation of cracks because the surveys were performed below the permanent water table. While partial saturation is a possibility, we do not have any information to estimate it. To estimate velocity for the uncracked matrix, we used velocities from laboratory measurements of intact basalt [Carmichael, 1982]; Vp = 7.5 km/s and Vs = 4.3 km/s.

The P- and S-wave velocity tomograms for the TAN-37 - TAN-25 well pair were used as estimates of cracked rock velocity to generate a crack density tomogram, Figure 11. The tomogram shows anomalous regions of high and low crack density, with two subhorizontal, high crack density zones between 70 and 80 m which may represent the hydrologic flow zones. The crack density calculation assumes all other material properties are constant. Therefor, variation in crack density will include any other changes in subsurface properties (including partial gas and DNAPL saturation) as estimated changes in crack density, potentially causing anomalous crack density results. While this method provides an estimate of rock properties, we do not believe that the equivalent media approach is the best method for obtaining hydrologically important rock properties for fractured basalt because the hydrologic flow is probably dominated

by discrete fractures and rubble zones rather than continuous matrix fracturing. Discrete fracture approaches (e.g. [Pyrak-Nolte, et al., 1990], and [Schoenberg and Sayers, 1995]) may provide better estimates of fracture properties, and future work will focus on these methods.

3.2.3. Guided Wave Observation and Analysis. As part of the orbital vibrator analysis, anomalous high amplitudes were observed near 74 m depth in the TAN-37 - TAN-25 data set. Figure 12 shows the seismograms for a zero offset profile (source and receiver at the same depth). In addition to showing the large variability of seismic response with depth, Figure 12 shows an anamolous high amplitude reverberant arrival at 73 - 75 m depth, with low amplitude arrivals above and below that depth range. We believe the high amplitude wave is a guided wave, a type of trapped energy observable in low velocity layers.

Guided waves were observed in coal seams in the early 1960's [Krey, 1963], motivating the development of techniques to generate and analize the waves for discontinuities in coal seams [Buchanan and Jackson, 1986]. The coal seam applications usually had access to the coal seam from mining works, and were therefore not strictly crosswell geometries. In oil and gas reservoirs, crosswell surveys have generated guided waves which were used for studying the continuity of horizons between wells ([Krohn, 1992] and [Lines, et al, 1992]). In fault zones, which are often approximated by vertical low velocity zones, "guided" or "trapped" waves have been observed [Li and Leary, 1990] and modeled [Ben-Zion, 1998]. Like fault zones, fracture zones are approximated by low velocity zones. Guided waves have been numerically modeled for an equivalent

anisotropic channel (a channel with aligned cracks) [Lou and Crampin, 1993], and for waveguides formed by two parallel discrete fractures [Nihei, et al, 1999].

Numerical modeling of the TAN guided wave seismograms using a finite difference solution of the acoustic wave equation (using the commercial software ProMAX) was performed to aid the guided wave interpretation. Initially, the tomographically derived velocity structure between wells TAN-37 and TAN-25 was used to model the data. This approach did accurately reproduce the first arrival times (as expected), however the guided wave was not accurately reproduced. We believe the low resolution of tomography for the orbital vibrator source did not image the distinct low velocity zone necessary for generation of guided waves.

Using velocities from the piezoelectric tomograms, we built a simplified 3 layer model with a low velocity layer, such as an interbed rubble zone, between high velocity regions typical of dense, unfractured basalt. Initially, modeling did not produce a guided wave. We lowered the velocity of the middle layer to create a better wave guide. The final velocities used were 4 km/s for dense basalt and 1.8 km/s for the rubble zone. The thickness of the low velocity zone was varied to find the best match between synthetic seismograms and recorded data for 5 recordings centered on 74 m. A good match was found for both 1.5 and 1.0 m thick low velocity layers, with the 1.0 m layer being best. Figure 13 shows these models in schematic form. A comparison of the recorded seismograms is shown in Figure 14. The match between recorded seismograms and numerically modeled seismograms is quite good, especially at 73.5 and 74 m. We believe this 3-layer numerical model concurs with the conceptual model of a fracture

zone with high hydraulic permeability within less fractured basalt. The existence of a hydrologically important flow zone at the depth of the guided wave (74 m) is supported by the piezoelectric data in Figure 5 which show a thin zone of low velocity and high attenuation at this depth. This interpretation is also supported by observation a distinct fracture zone in the borehole televiewer data from well TAN-37. Therefore, we believe the guided wave is defining a thin, hydrologically significant zone within the basalt flows.

We also modeled the effect of "blockages" of the low velocity zone, as if a lens of dense basalt interrupted the rubble zone (Figure 13). Our results show that intersection of a rubble zone by the boreholes is an important factor. Blockage between wells caused a delayed arrival time for the guided wave (because of the intervening high velocity media), while a blockage at either well caused large changes in waveform. Figure 15 shows the effect of a 6 m wide blockage at one well (model 2.5 in Figures 13 and 15). The blockage model data had a clear time shift compared to the field data and the unblocked model (compare Figures 14 and 15). This finding implies that fracture zone guided waves could be used to infer details of hydrologically important subsurface features.

4. Conclusions

We have successfully obtained crosswell seismic data in a fractured basalt aquifer at the INEEL TAN site. The fractured basalt lithology of INEEL's TAN site (with possible sedimentary interbeds) provides a difficult media for seismic profiling. However,

we have acquired multiple high frequency P-wave data sets in close well spacings (less than 25 m) with a piezoelectric seismic source. We have used an orbital vibrator seismic source to acquire P- and S-wave data sets in larger well spacings (nearly 40 m), with P-waves recorded at nearly 60 m well spacing. The use of the orbital vibrator with a hydrophone array successfully demonstrated the applicability of a this new type of seismic source for environmental applications needing P- and S-wave measurements. Travel time tomography was accomplished for both P- and S-wave data sets. From these tomograms, Vp/Vs ratio and other rock properties can be calculated. The direct subsurface measurement of these ratios is very useful for understanding material properties.

In general, at the fractured basalt TAN site, regions of slow seismic velocity are found to correspond with zones of contaminant transport (and by inference higher permeability and increased fracturing). Regions of low amplitude (high attenuation) also appear to correspond with zones of permeability. Regions of anomalously high attenuation, such that tomography could not be achieved between certain wells, may indicate other factors such as DNAPL concentration or partial gas saturation are affecting wave propagation at the TAN site.

Within the tomograms generated, we believe horizontal fracture/rubble zones between basalt flows are causing the drop in seismic velocity, and are paths for fluid flow. The permeable zones as determined from well logs, borehole televiewer and hydrologic modeling correspond to low velocity in the tomograms. The lower resolution orbital vibrator tomograms show the significant hydrologic separation of the upper and lower

sections of the aquifer. This scale of resolution (10-15 m) corresponds to the TAN site hydrologic modeling using an equivalent porous medium. The higher resolution of the piezoelectric tomograms is much greater than the resolution of the large scale hydrologic modeling used for remediation at the TAN site.

High amplitude guided waves were observed and were coincident with an interpreted contaminant flow-zone. We believe the guided waves are caused by low velocity zones and define the thickness of the zone within 1- 2 m. This analysis provides much better resolution than velocity tomograms for the orbital vibrator source. Fracture-zone guided waves could provide a useful tool for understanding other fractured aquifers.

The combination of piezoelectric data for closer well spacing and orbital vibrator for larger well spacings has provided optimal imaging capability and has been instrumental in understanding the TAN site aquifer's hydrologic properties and their scale lengths.

5. ACKNOWLEDGMENTS

This work was supported by the Environmental Management Science Program (EMSP) of the U.S. Department of Energy under contract no. DE-AC03-76SF000098. Data processing was performed at the Center for Computational Seismology which is supported by the Director, Office of Energy Research, Office of Basic Energy Sciences, of the U.S. Department of Energy under contract No. DE-AC03-76SF000098. Assistance at INEEL provided by Tom Wood, Chad Hersley, Rick Colwell and John Bukowski. The authors would like to thank Tom Wood of INEL and Ken Williams and Don Lippert of LBNL for assisting data acquisition during a cold Idaho winter.

References

Ben-Zion, Yehuda, Properties of seismic fault zone waves and their utility for imaging low-velocity structures, *Jour. of Geophy. Res.*, 103, B6, 12567-12585, 1998.

Buchanan, D.J., and L.J. Jackson, The in-seam seismic method, in *Coal Geophysics*, Geophysics Reprint No. 6, edited by D.J. Buchanan and L.J. Jackson, pp275-277, Soc.Explor. Geophys., Tulsa, OK, 1986.

Bukowski, J.M., Bullock, H., and Neher, E.R., 1998, Site Conceptual Model: 1997 Activities, Data Analysis, and Interpretation for Test Area North, Operable Unit 1-07B, Idaho National Engineering and Environmental Laboratory Report INEEL/EXT-98-00575.

Bukowski, J.M., and Sorenson Jr, K.S., 1998, Site Conceptual Model: 1996 Activities, Data Analysis, and Interpretation for Test Area North, Operable Unit 1-07B, Idaho National Engineering and Environmental Laboratory Report INEEL/EXT-97-00556.

Carmichael, 1982, editor, Handbook of Physical Properties of Rocks Volume II, CRC Press, Inc.

Cicerone, R. D. and Toksoz, M. N., 1995, Fracture characterization from vertical seismic profiling data, *Journal of Geophysical Research*, 100, p4131-4148.

Cao, S. and Greenhalgh, S., 1997, Cross-well seismic tomographic delineation of mineralization in a hard rock environment, *Geophysical Prospecting*, 45, p449-460.

Daley, T.M.,and Cox D., 1999, P- and S-wave seismic crosswell profiling with an orbital vibrator, *Geophysics* (to be published in 2001), Lawrence Berkeley National Laboratory Report LBNL- 43070, Berkeley CA, March 1999.

Geller, J. T., and Myer, L. R., 1995, Ultrasonic imaging of organic liquid contaminants in unconsolidated porous media, *Journal of Contaminant Hydrology*, 19, p85-104.

Harris, J.M., Nolen-Hoeksema, R.C., Langan, R.T., Van Schaack, Lazaratos, S.K., Rector, J.W.III, 1995, High-resolution crosswell imaging of a west Texas carbonate reservoir: Part 1 - Project summary and interpretation, *Geophysics*, 60, 667-681.

Lines, L. R., Kelly, K. R., Queen, J., 1992, Channel waves in cross-borehole data, *Geophysics*, 57, p334-342.

Krey, T. C., 1963, Channel waves as a tool of applied geophysics in coal mining, *Geophysics*, 28, p701-714.

Krohn, C. E., 1992, Cross-well continuity logging using guided seismic waves, *The Leading Edge*, 6, p39.

Li, Y.G. and P. Leary, Fault zone seismic trapped waves, *Bull. Seismol. Soc. Am.*, 80, 1245-1271, 1990.

Lou, M. and Crampin, S., 1993, Modeling guided waves in cross-hole surveys in uncracked and cracked rock, *Geopysical Prospecting*, 41, p241-265.

Mason, I.M., 1981, Algebraic reconstruction of a two-dimensional velocity inhomogeneity in the High Hazles seam of Thoresby colliery, *Geophysics* , 46, p298.

Nihei, K. T., Yi, W., Myer, L. R., Cook, N.G.W., and Schoenberg, M., 1999, Fracture Channel Waves, *Journal of Geophysical Research*, 104, p4769-4781.

O'Connell, R.J., and Budiansky, B., Seismic Velocities in Dry and Saturated Cracked Solids, *Journal of Geophysical Research*, 79, n35, p5412-5426.

Peterson, J.E., Paulsson, B.N.P., and McEvilly, T.V., 1985, Applications of algebraic reconstruction techniques to crosshole seismic data, *Geophysics*, 50, p1566-1580.

Pyrak-Nolte, L.J., Myer, L.R., and Cook, N.G.W, 1990. Anisotropy in Seismic Velocities and Amplitudes from Multiple Parallel Fractures, *Journal of Geophysical Research*, 95, nB7, p11345-11358.

Rector, J.W.III, Lazaratos, S.K, Harris, J.M., Van Schaack, M, 1995, High-resolution crosswell imaging of a west Texas carbonate reservoir: Part 3 - Wavefield separation of reflections, *Geophysics*, 60,692-701.

Rector, J.W. III, editor, Special Issue: Crosswell Methods, *Geophysics*, 60, n3.

Schoenberg, M., and Sayers, C. M., 1995, Seismic anisotropy of fractured rock, *Geophysics*, 60, p204-211.

Sorenson Jr., K.S., Wylie, A.H., Wood, T.R., 1996, Test Area North Site Conceptual Model and Proposed Hydrogeologic Studies, Operable Unit 1-07B, Idaho National Engineering Laboratory Report INEL-96/0105.

Vasco, D.W., Peterson, J.E., and Majer, E.L., 1996, A simultaneous inversion of seismic traveltimes and amplitudes for velocity and attenuation, *Geophysics*, 61, p1738.

White, J.E., Seismic waves: radiation, transmission, attenuation, McGraw Hill, Inc 1965.

Whitehead, R.L., Geohydrologic Framework of the Snake River Plain Regional Aquifer System, Idaho and Eastern Oregon, U.S. Geological Survey Professional Paper 1408-B, 1992.

T.M. Daley, E.L. Majer, and J.E. Peterson, all at Center for Computational Seismology, Lawrence Berkeley National Laboratory Berkeley, CA

Received _____

LBNL Research Report LBNL-45533

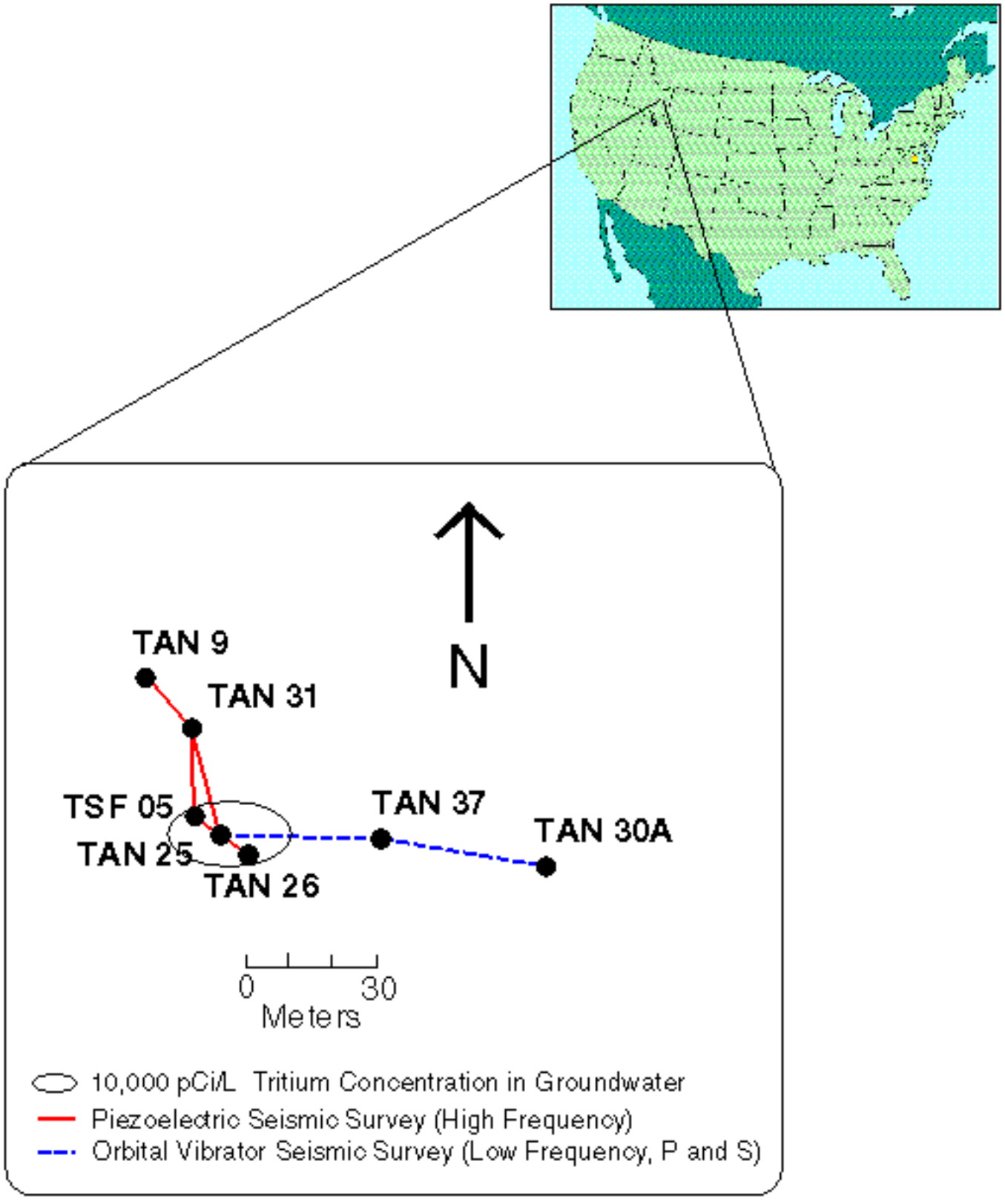

Figure 1 Well locations at the INEEL TAN site in Idaho. Contaminant concentration contour is approximate. Other attempted crosswell surveys are not shown.

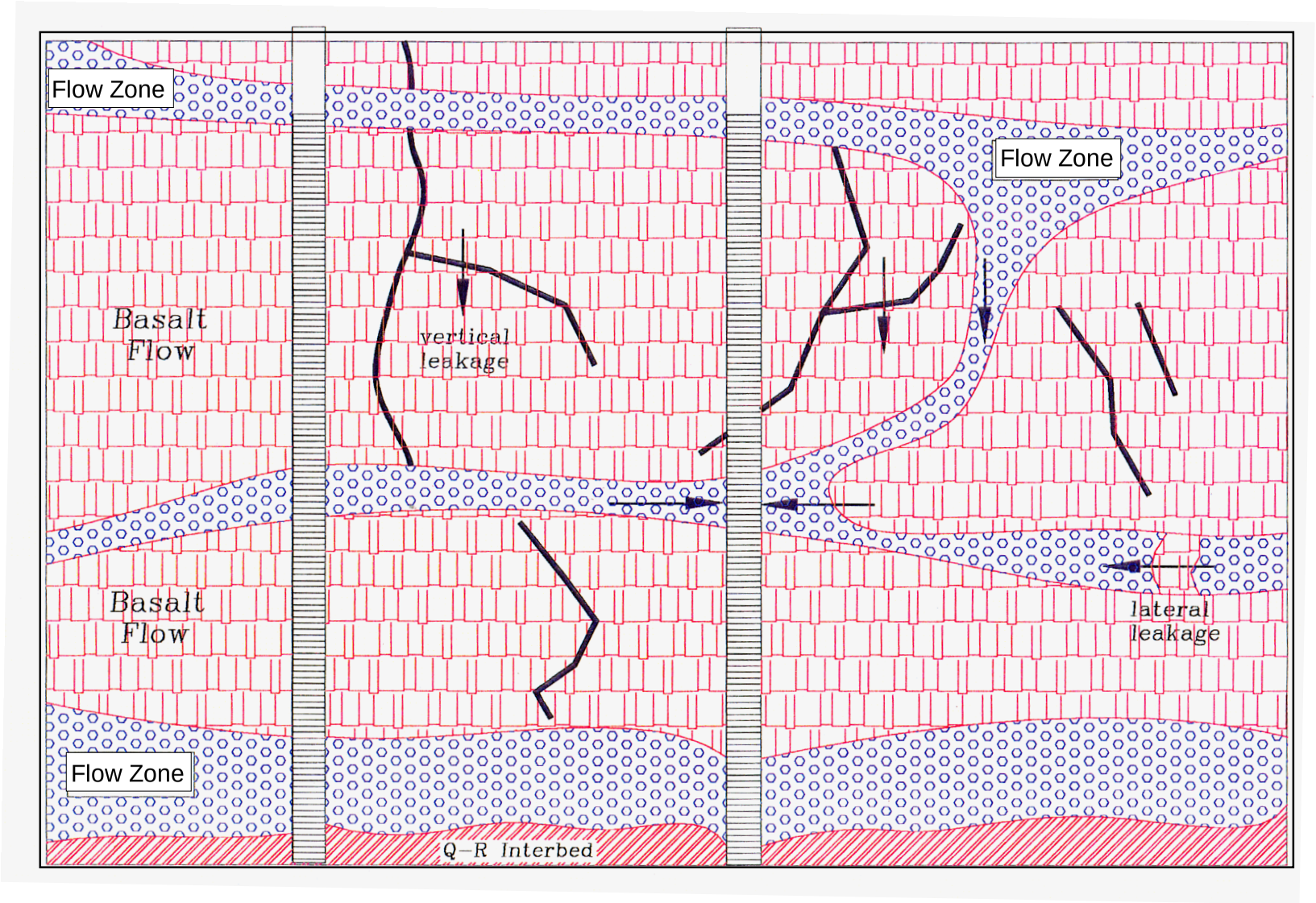

Figure 2 Conceptual model of hydrologic flow within the aquifer at the INEEL TAN site. A sequence of thin basalt flows contain mainly horizontal flow zones with vertical leakage between zones. These zones are believed to be interbed basalt rubble zones. Sedimentary Interbeds (e.g. Q-R) can act as a barrier to vertical flow. Figure taken from Bukowski, et al., 1998.

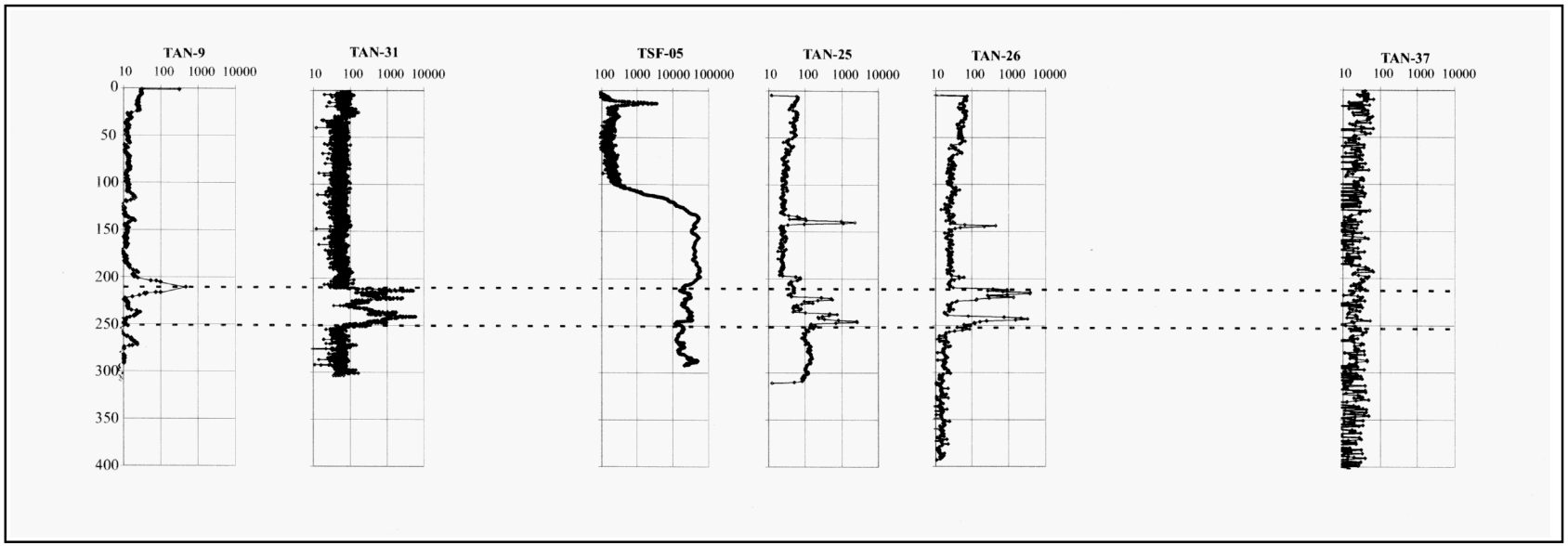

Figure 3 Gamma logs from tomography wells at the INEEL TAN site. Gamma count is dominated by radionuclide contamination in the groundwater. High gamma counts correlated between wells (inside dashed lines) show zones of contaminant flow within the aquifer. These zones are imaged by seismic tomography as low velocity zones.

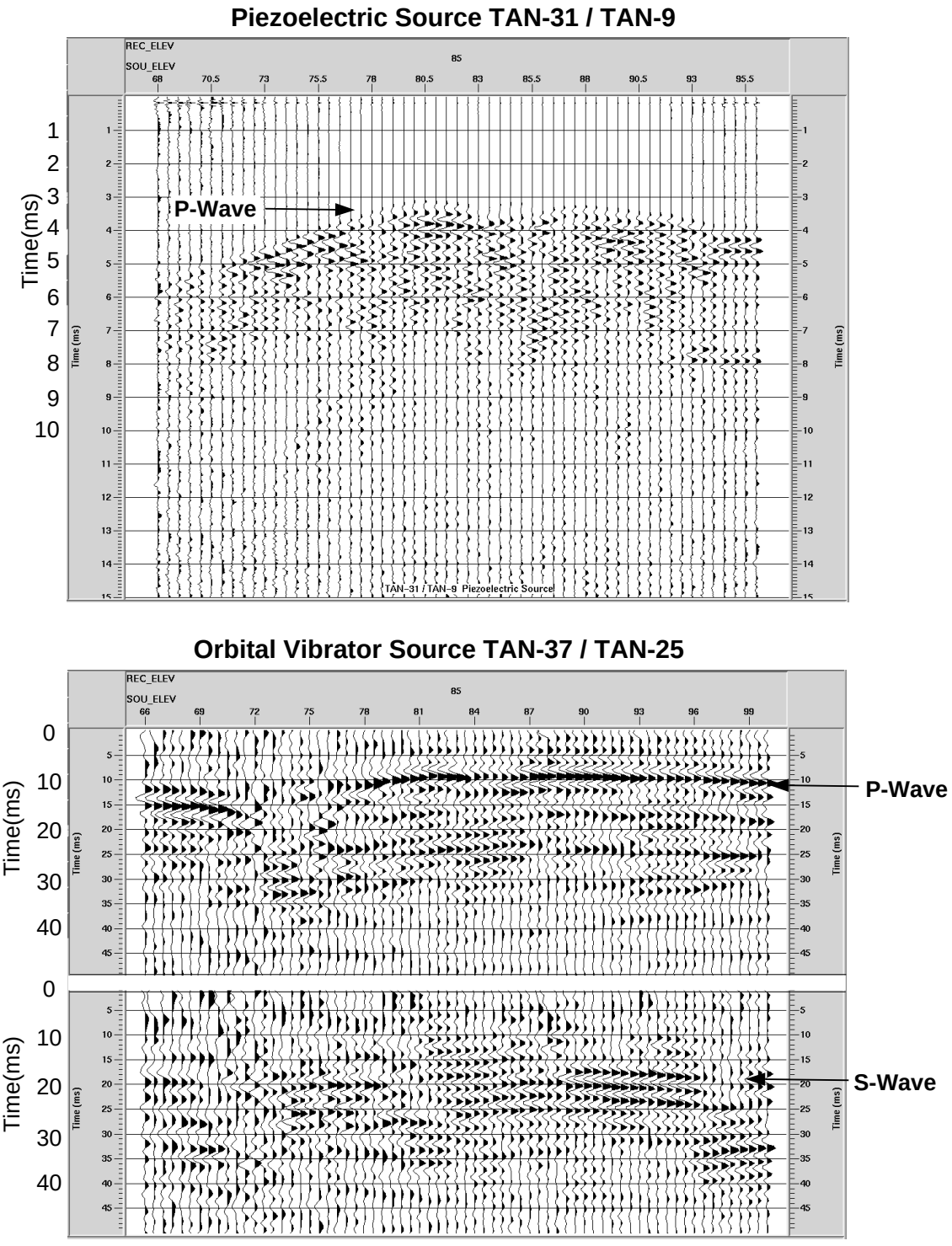

Figure 4a (top) and 4b (bottom) Receiver gathers for the two seismic sources. The receiver depth is 85 m, the source depths are 66 to 100 m. The orbital vibrator data (bottom) contains in-line (P-wave) and cross-line (S-wave) components.

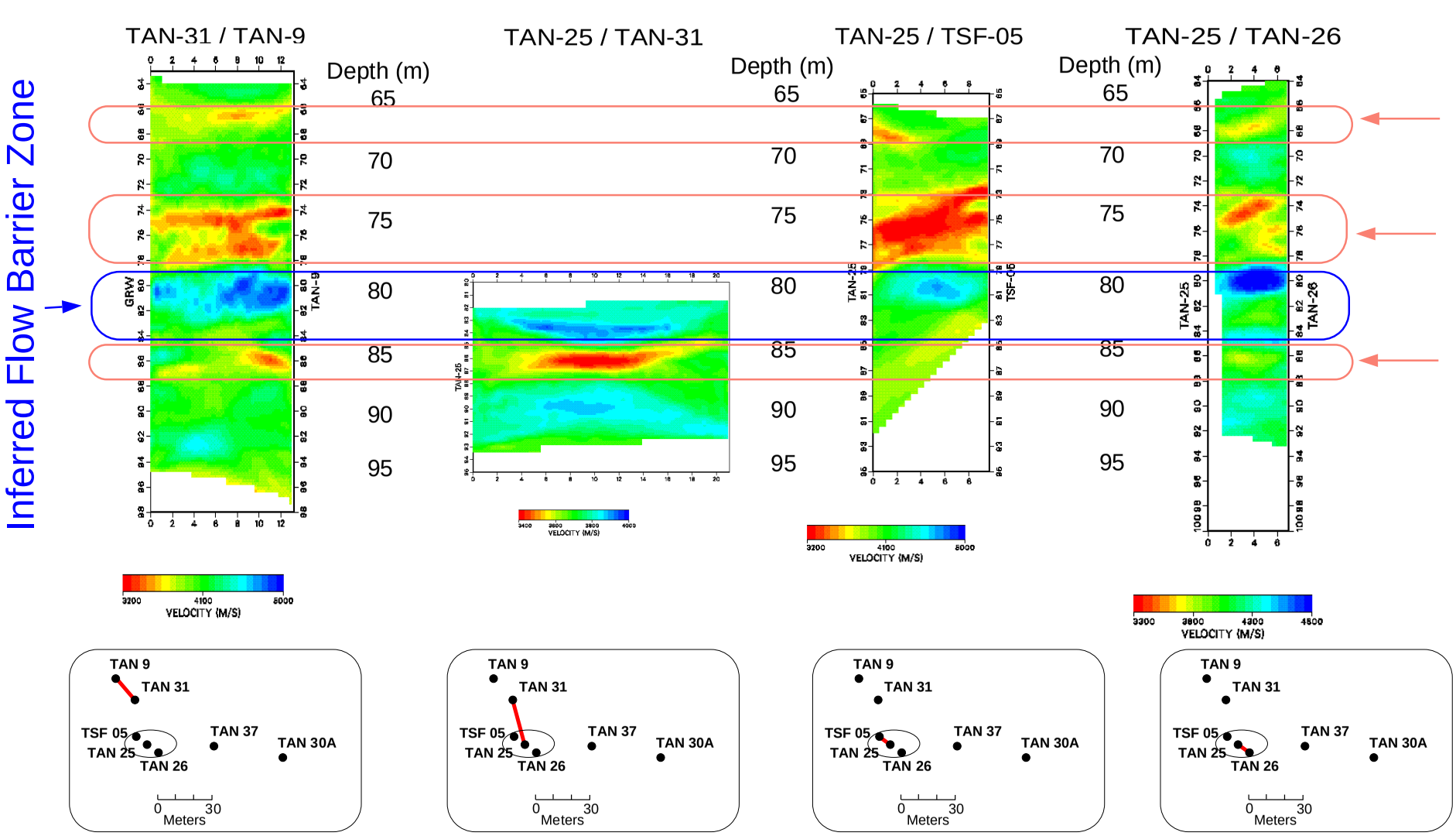

Figure 5 Seismic velocity tomograms (top) from the INEEL TAN site with location map (bottom) showing well pair. Zones of low velocity (yellow - red) are interpreted as fractured basalt (possibly rubblized contacts between basalt flows) which allow high flow within the aquifer. High velocity zones (blue) are interpreted as dense, unfractured basalt which acts as a barrier to contaminant flow within the aquifer. The upper two inferred flow zones have been confirmed as contaminant transport zones by well logs.

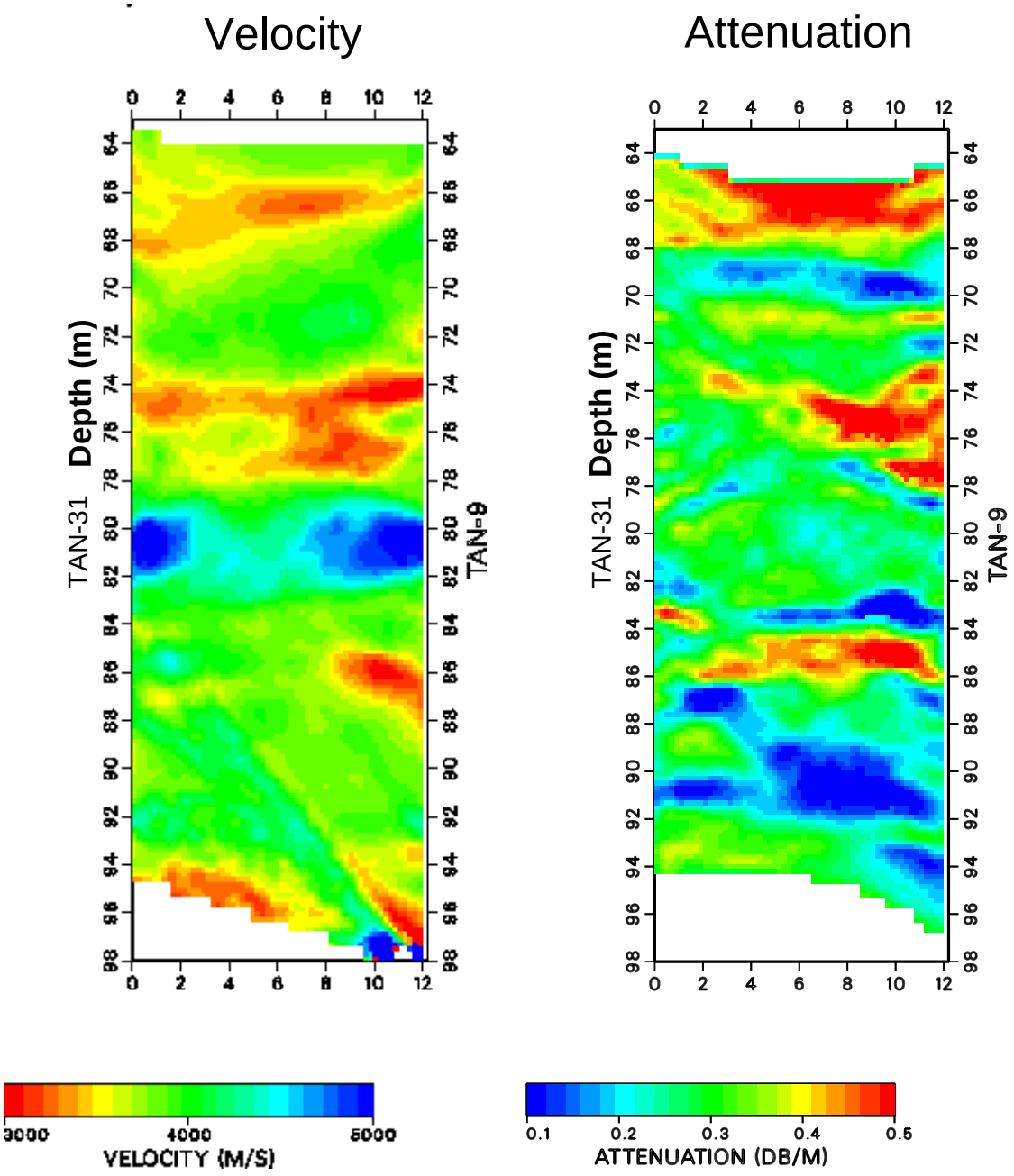

Figure 6 Seismic tomographic inversion results for well pair TAN-31 / TAN-9. This data used the high frequency piezoelectric source giving 1- 2 m resolution. Zones of low velocity and high attenuation (such as 73 - 76 m, and 65 - 67 m) are interpreted as fracture zones which provide fluid flow zones for contaminant transport.

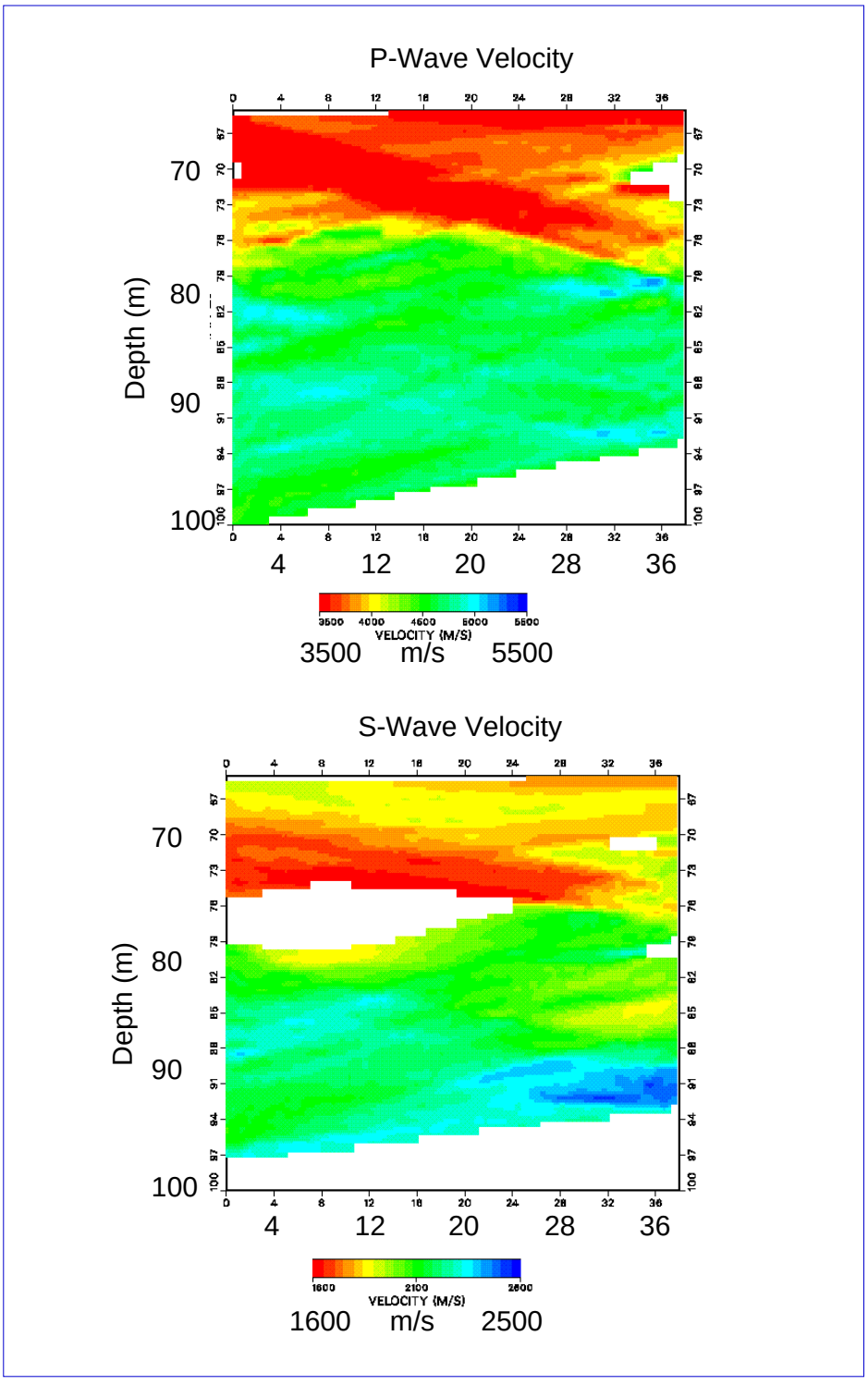

Figure 7 P-wave (top) and S-wave (bottom) velocity tomograms for data acquired with orbital vibrator source at the INEEL TAN site between wells TAN-25 and TAN-37. The low velocity region between 65 and 80 m corresponds with higher flow in the basalt aquifer.

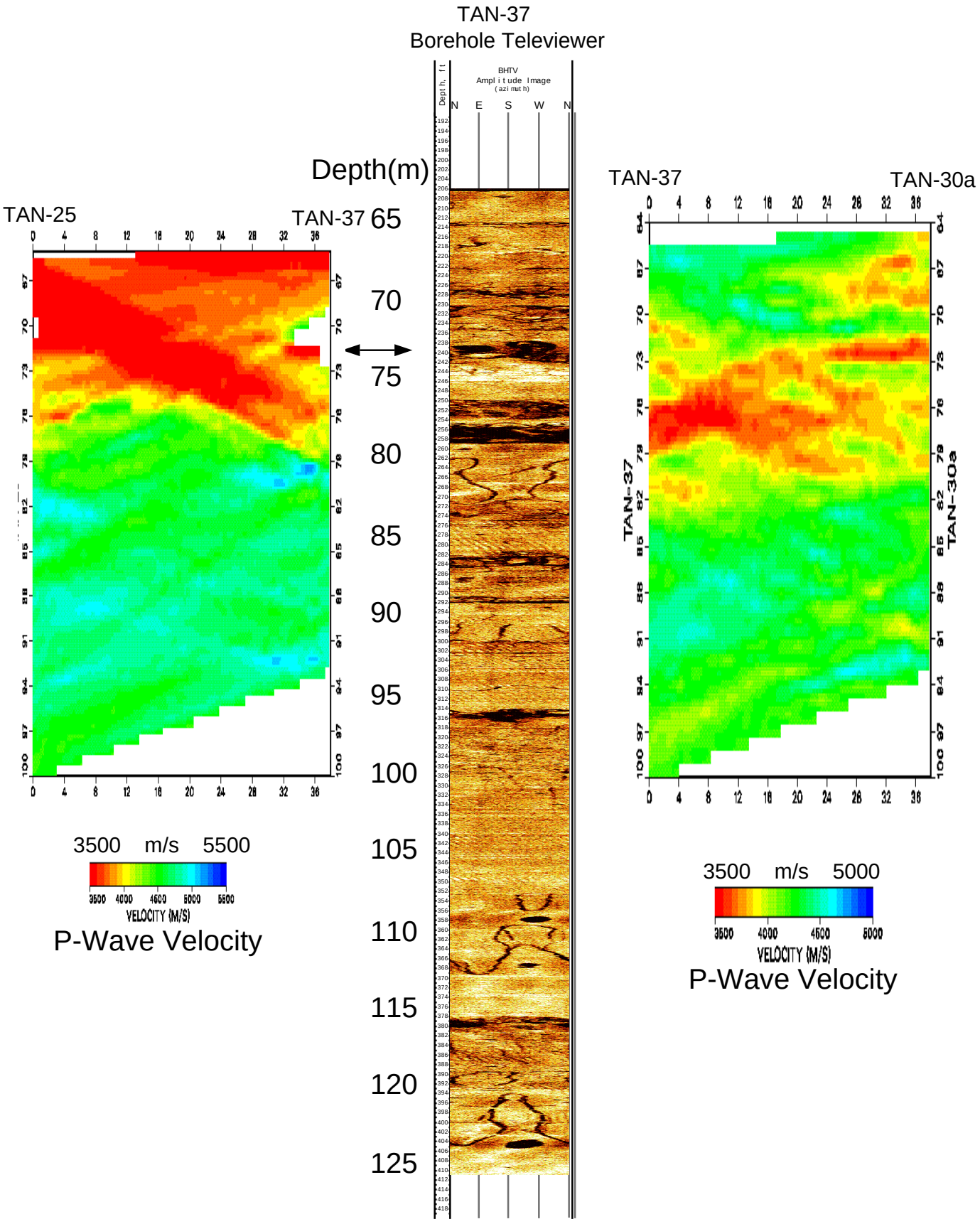

Figure 8 TAN site P-wave seismic tomography (wells 25 and 37 left; wells 37 and 30a right) along with borehole televiewer (center). Regions of low velocity (red to yellow) above 80 m depth define the regions of fracture flow and contaminant transport. Arrow at 74 m indicates depth of observed fracture zone seismic guided wave which indicates fracture connectivity between wells.

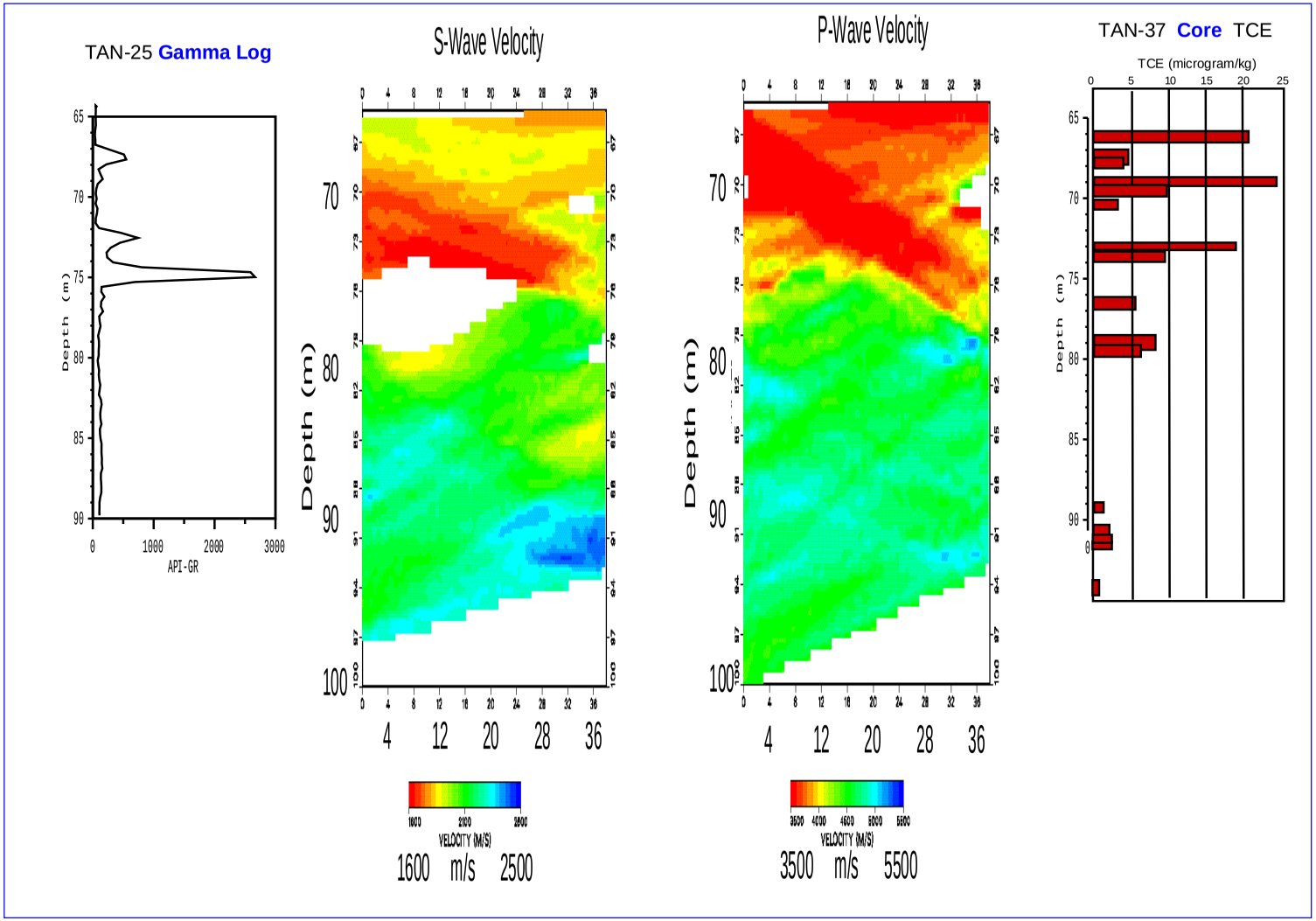

Figure 9 Comparison of contaminant sampling in boreholes and croswell velocity tomogram. TAN-25 Gamma Log (left) indicates presence of radionuclide contamination. TAN-37 TCE contamination from core measurement (right) indicates TCE concentration. Seismic S-Wave and P-Wave velocity (center) indicates more fractured rock as low velocity (red to green) and less fractured rock as high velocity (green to blue). The 65 to 80 m depth zone has low velocity and increased contaminants, showing the relation between fracture flow and fracture induced seismic velocity variation.

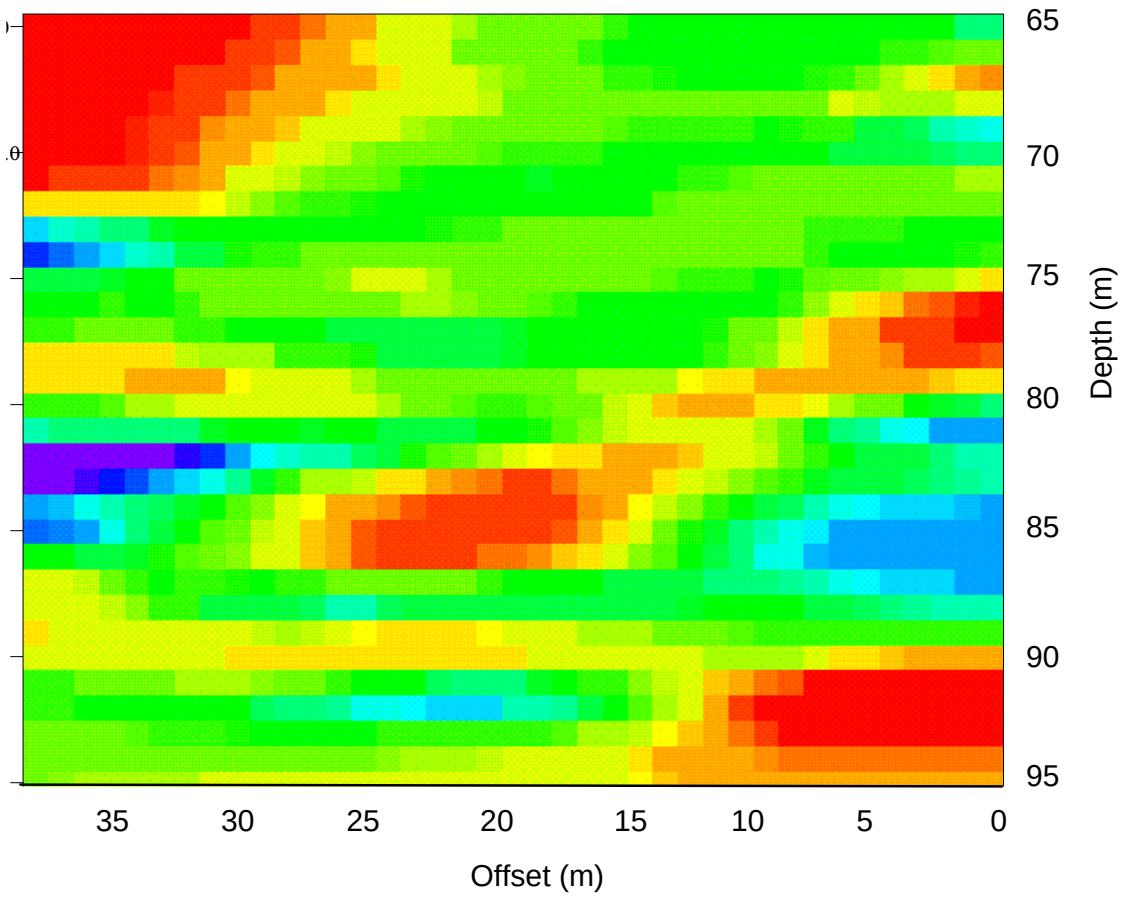

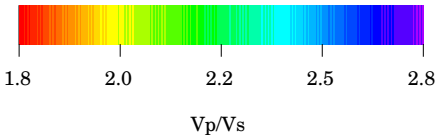

Figure 10 Display of Vp/Vs velocity ratio for the tomographic velocities between wells TAN-37 and TAN-25.

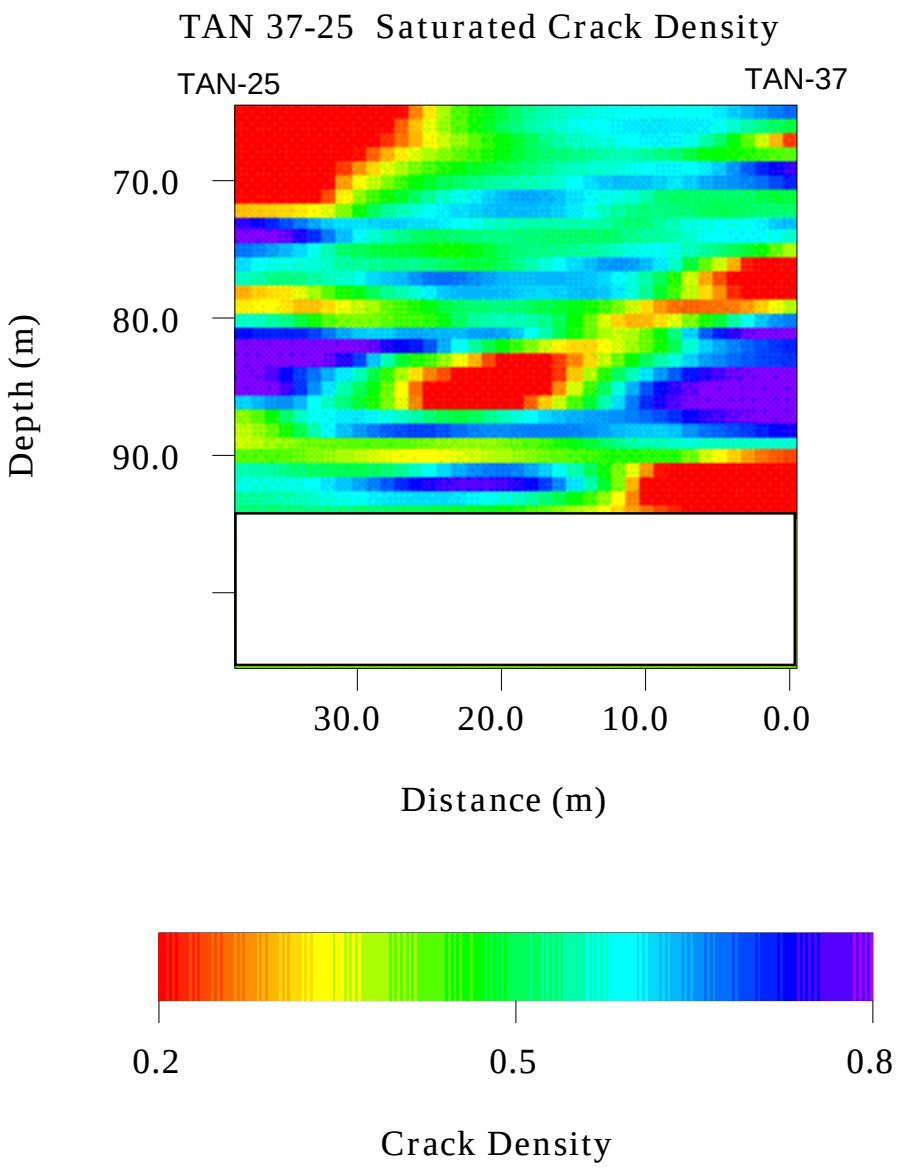

Figure 11 Crack density (dimensionless) calculated from P- and S-wave tomographic velocities. All other material properties are assumed to be constant and cracks are assumed to be fully saturated.

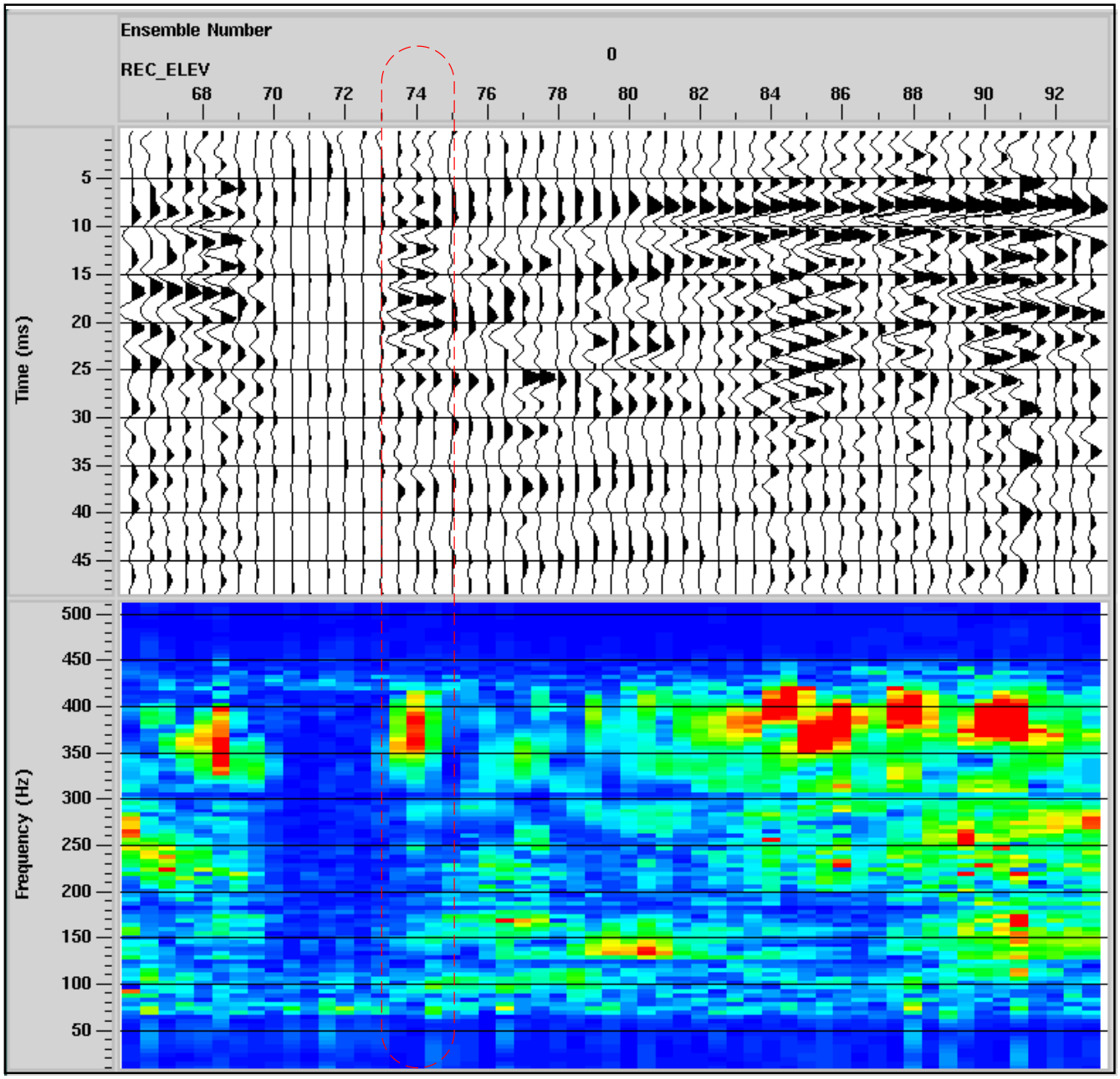

Figure 12 Zero offset profile (source and receiver at the same depth) for the TAN-37 / TAN-25 well pair. Depth in meters is labeled at top as REC_ELEV. Seismograms (top) and spectra (bottom) show large variability. The zone in the dashed lines is interpreted as a guided wave with large amplitude at 74 m depth and peak spectra (yellow to red colors) between 350 and 400 Hz.

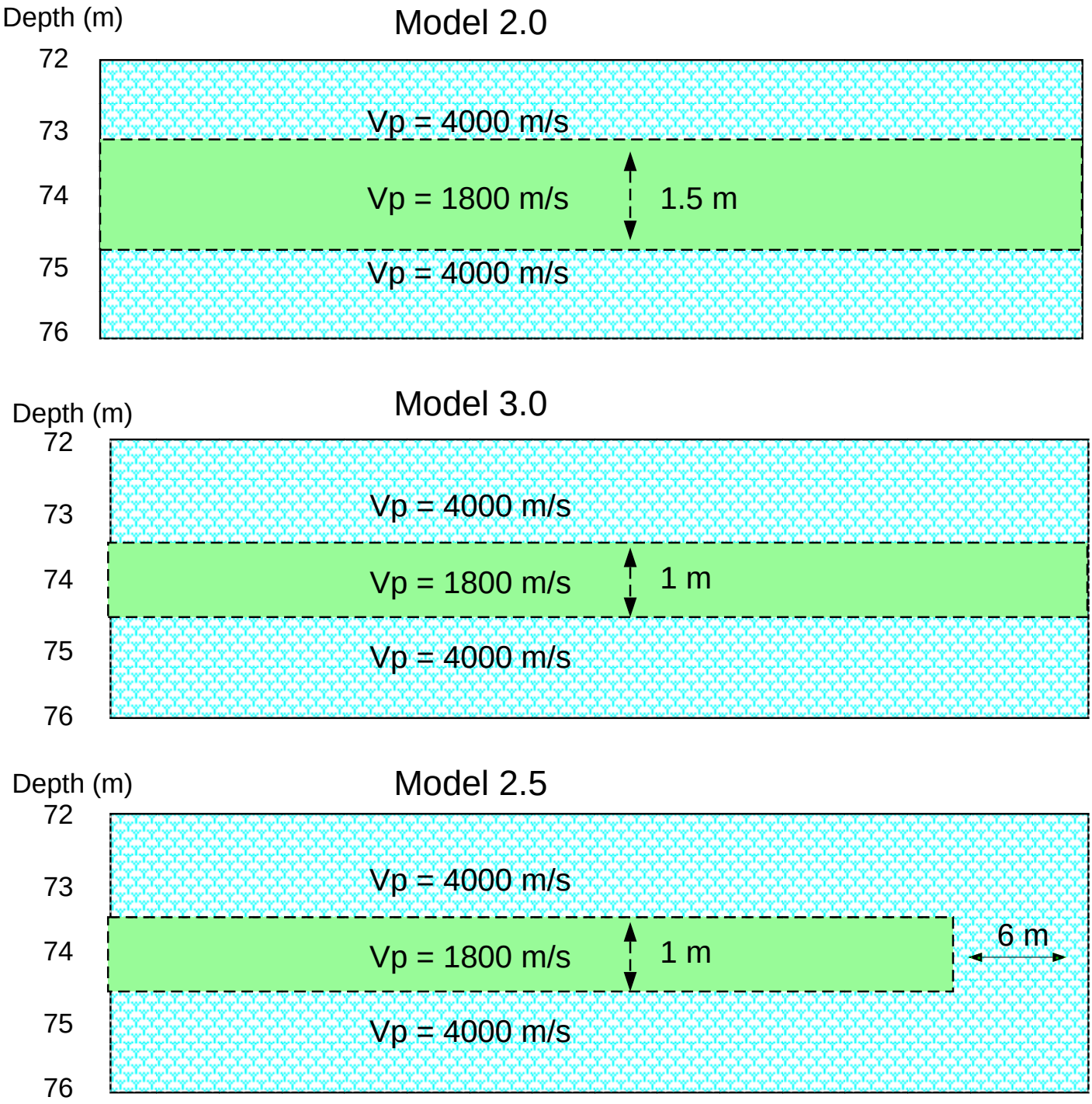

Figure 13 Velocity models used for finite difference seismic modeling of guided wave observed in TAN-37 / TAN-25 well pair. 4000 m/s material represents unfractured, low permeability bsalt, 1800 m/s represents fractured, rubble zone basalt.

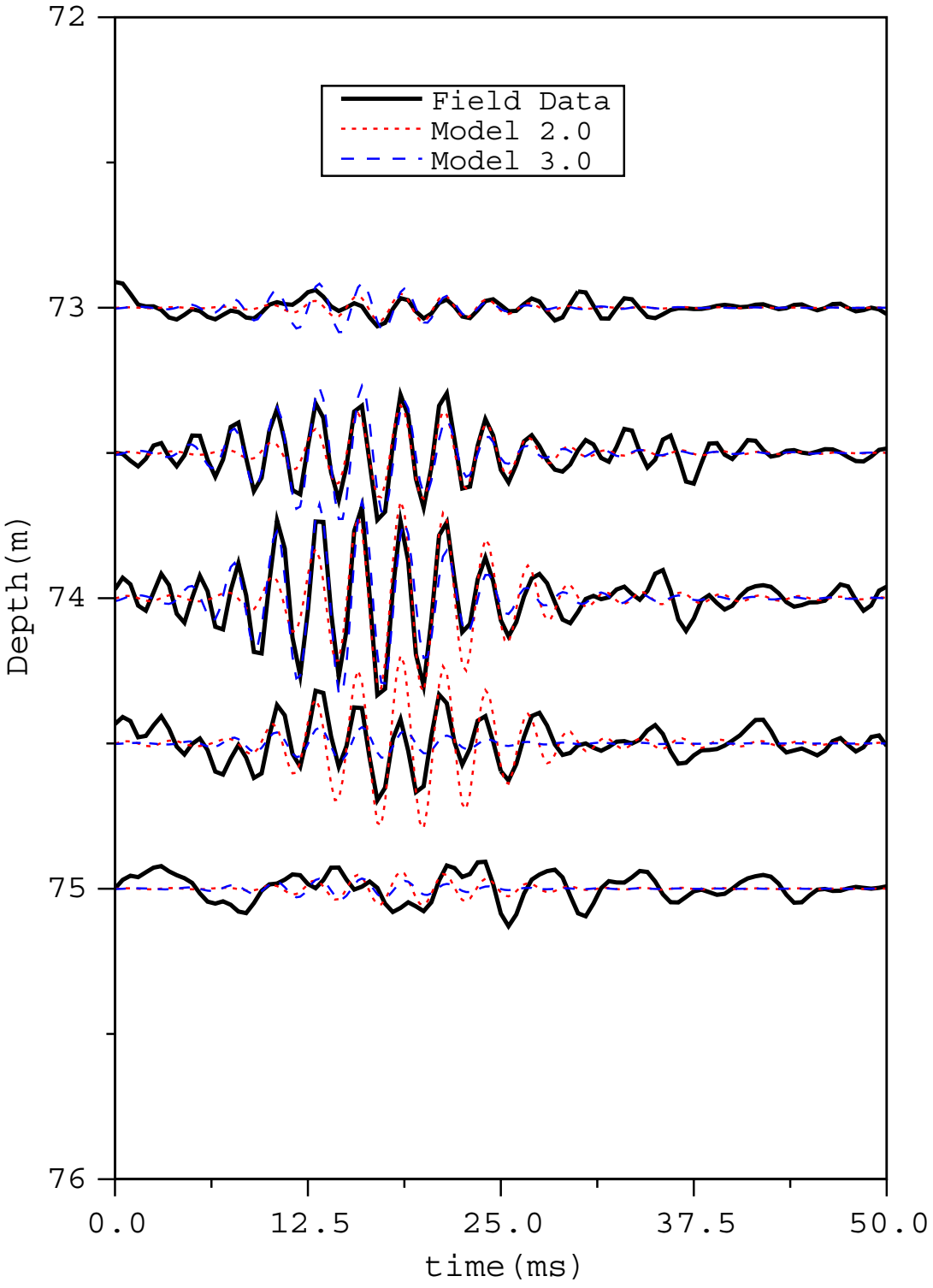

Figure 14 Comparison of modeled and field data for guided wave at TAN site. Model 2.0 is a 1.5 m thick low velocity zone, while model 3.0 is a 1.0 m thick low velocity zone. The low velocity material is 1800 m/s surrounded by 4000 m/s material.

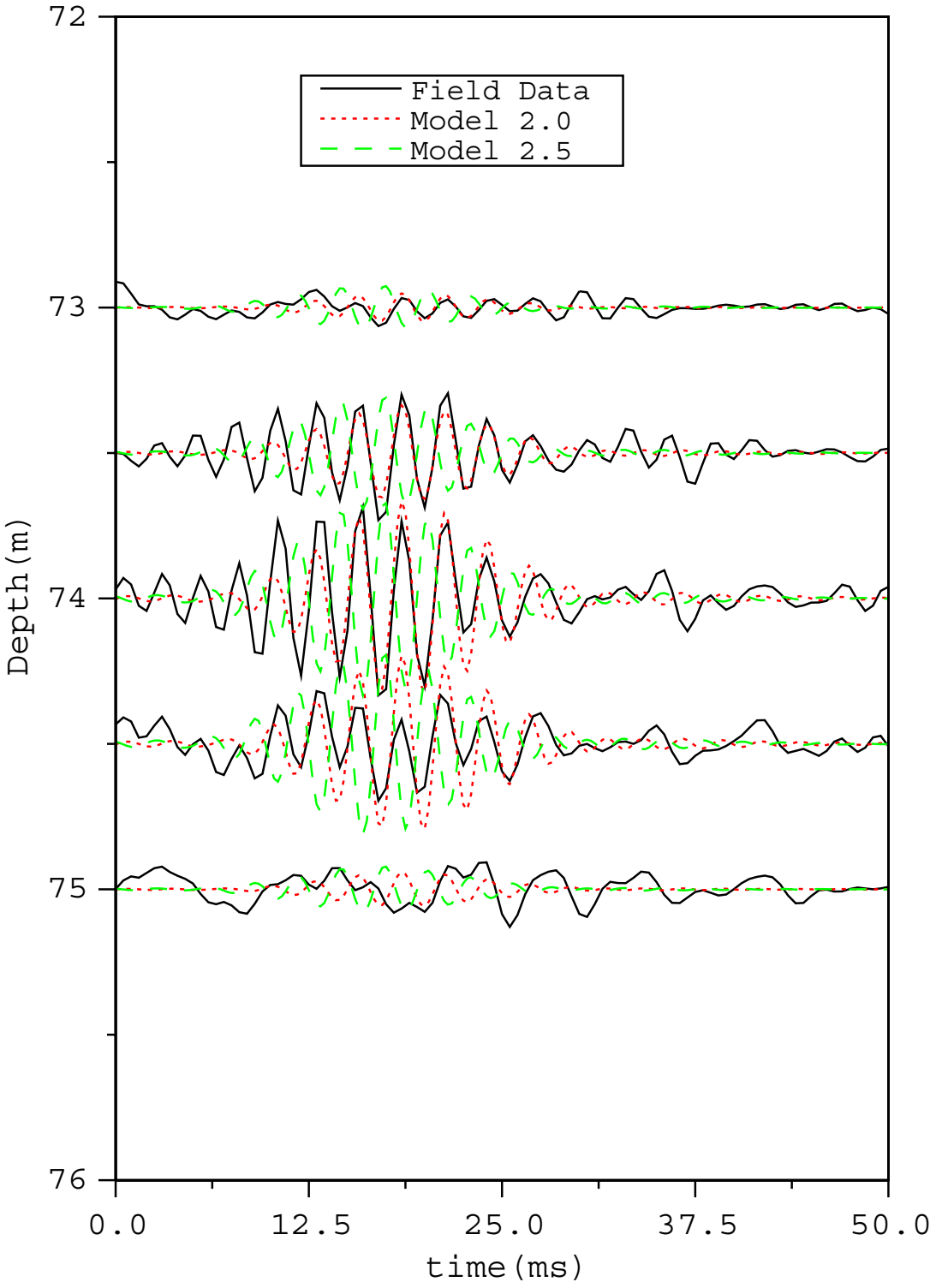

Figure 15 Comparison of two models and field data for guided wave at TAN site. Model 2.0 is a 1.5 m thick low velocity zone. Model 2.5 has the same low velocity zone, but the low velocity is not continuous between wells. In model 2.5, the high-velocity portion (representing unfractured basalt which acts as a barrier to flow) is 6 m of the 38 m well separation.